scientific reports

Check for updates

OPEN

Cycloastragenol attenuates osteoarthritis by restoring chondrocyte senescence via the NRF2/NF-κB signaling axis

Shuhao Zhang[1,3], Yanlong Zou[1,3], Jundong Long[1], Yufan Wang[1], Jian Chen[1]✉ & Miao Teng[2]✉

Osteoarthritis (OA) involves oxidative stress-induced chondrocyte senescence and extracellular matrix (ECM) dysregulation, yet disease-modifying therapies remain elusive. This study investigates the effects of cycloastragenol (CAG), a telomerase-activating triterpenoid from Astragalus membranaceus, on OA progression with a focus on NRF2/NF-κB signaling. In vitro, CAG suppressed oxidative stress-induced senescence in primary rat chondrocytes, evidenced by reduced SA-β-gal positivity, partially restored EdU proliferation, and downregulated senescence related proteins expression. In addition, CAG concurrently attenuated senescence-associated secretory phenotype (SASP) and partially restored ECM homeostasis. Mechanistically, molecular docking analysis suggested a potential interaction between CAG and the Kelch domain of KEAP1. Consistent with this, CAG treatment was associated with NRF2 pathway activation and attenuation of TBHP-induced NF-κB signaling. Importantly, genetic inhibition of NRF2 significantly attenuated the protective effects of CAG, supporting a required role for NRF2 in mediating CAG-induced suppression of oxidative stress and inflammatory signaling. In vivo, intra-articular CAG administration in monosodium iodoacetate (MIA)-induced OA rats reduced cartilage degradation, rescued ECM homeostasis, and enhanced NRF2 activation. Collectively, CAG mitigates the degradation of the extracellular matrix and suppresses the senescence-associated secretory phenotype (SASP) induced by osteoarthritis (OA).

Keywords Cycloastragenol, Osteoarthritis, Oxidative stress, NRF2, Senescence-associated secretory phenotype

Abbreviations

ACAN	Aggrecan
ADAMTS5	A disintegrin and metalloproteinase with thrombospondin motifs 5
CAG	Cycloastragenol
COL2A1	Collagen type II alpha 1 chain
CCK8	Cell counting kit-8
ECM	Extracellular matrix
KEAP1	Kelch-like ECH-associated protein 1
IL-6	Interleukin-6
IL-1β	Interleukin-1β
MIA	Monosodium iodoacetate
MMP	Metalloproteinase
H&E	Hematoxylin and eosin
NRF2	NFE2 Like BZIP transcription factor 2
NF-κB	Nuclear factor kappa B
OA	Osteoarthritis
OARSI	Osteoarthritis Research Society International
PBS	Phosphate-buffered saline
PVDF	Poly(vinylidene fluoride)
ROS	Reactive oxygen species

[1]Department of Plastic and Cosmetic, Yubei Hospital, Chongqing 401120, China. [2]Department of Plastic and Cosmetic, Shenzhen Qianhai Taikang Hospital, Shenzhen 518054, China. [3]Shuhao Zhang and Yanlong Zou contributed equally to this work. ✉email: jianchen0022@126.com; mteng1978@163.com

S-O	Safranin O-fast green
SASP	Senescence-associated secretory phenotype
SA-β-gal	Senescence-associated β-galactosidase
SVF	Stromal vascular fraction
TNF-α	Tumor necrosis factor-alpha
TMB	Tetramethylbenzidine
TBHP	*Tert*-Butyl hydroperoxide
TERT	Telomerase reverse transcriptase

Osteoarthritis (OA), the most prevalent degenerative musculoskeletal disorder worldwide, affects approximately 7.6% of the global population[1,2]. With accelerating population aging, the number of individuals suffering from knee OA is projected to rise by 74.9% by 2050, imposing escalating socioeconomic burdens—annual OA-related healthcare expenditures in the United States alone exceed $80 billion[1,3]. Clinically, OA manifests as progressive joint pain, mobility restriction, and functional impairment, culminating in irreversible joint dysfunction[4]. Notably, current therapies fail to halt or reverse early-stage degenerative changes, leaving invasive surgical interventions as the sole option for advanced cases[4,5]. Pathologically, OA is characterized by disrupted articular cartilage homeostasis. Healthy cartilage comprises chondrocytes and their precisely regulated extracellular matrix (ECM)[6]. During OA progression, persistent inflammatory microenvironments and oxidative stress drive pathological chondrocyte alterations, including senescence and apoptosis[7,8]. These dysfunctional chondrocytes further secrete matrix metalloproteinases (MMPs), accelerating ECM degradation[9]. Consequently, developing novel strategies to restore chondrocyte homeostasis and ECM metabolic balance represents a critical scientific challenge in OA research.

Cellular senescence, a hallmark of OA progression, exhibits a strong positive correlation with disease severity[10]. Senescent chondrocytes display irreversible cell cycle arrest mediated by p53 overexpression and p16INK4a/p21CIP1 pathway activation, coupled with the senescence-associated secretory phenotype (SASP)[10]. SASP components—including pro-inflammatory cytokines and matrix-degrading proteins—exacerbate synovial inflammation, cartilage matrix breakdown, and synovial fibrosis through paracrine mechanisms[10,11]. Studies demonstrate that SASP-derived factors critically degrade type II collagen and aggrecan, while hyperactivated NF-κB signaling amplifies SASP-mediated pro-inflammatory effects[10,11]. Oxidative stress serves as a key instigator of chondrocyte senescence. Excessive reactive oxygen species (ROS) accumulation triggers senescence via DNA damage, telomere attrition, and epigenetic modifications[12,13]. In OA models, ROS induce redox imbalance while activating NF-κB-mediated inflammatory cascades, establishing a self-reinforcing "oxidative stress-inflammation-matrix degradation" cycle[12]. Within this context, the transcription factor NRF2 emerges as a pivotal regulator. As the master orchestrator of antioxidant defenses, NRF2 dissociates from KEAP1 under oxidative stress, translocates to the nucleus, and initiates antioxidant gene transcription[14,15]. Thus, targeting NRF2 to disrupt the oxidative stress-inflammation axis may offer a disease-modifying therapeutic strategy for OA[16,17].

Cycloastragenol (CAG), a triterpenoid derived from the hydrolysis of traditional Chinese herb *Astragalus membranaceus*, is one of the known natural compound capable of activating human telomerase[18–21]. Recent studies reveal its multimodal anti-aging properties: under hyperglycemic stress, CAG protects nucleus pulposus cells from metabolic injury and promotes proliferation[20]. Notably, CAG exhibits potent antioxidant effects through ROS scavenging and oxidative stress pathway modulation, underpinning its therapeutic potential for degenerative diseases[22,23]. Our study demonstrates that CAG suppresses SASP production and ameliorates ECM metabolic imbalance in chondrocytes, likely via targeted regulation of the NRF2/NF-κB signaling axis.

Results

CAG attenuates oxidative stress-induced chondrocyte senescence

Oxidative stress, a pivotal driver of osteoarthritis progression, disrupts chondrocyte redox homeostasis and energy metabolism, ultimately triggering cellular senescence cascades[24]. To investigate the therapeutic potential of CAG, we systematically evaluated its effects on TBHP-induced chondrocyte senescence[12,25,26]. The chemical structure of CAG is depicted in Fig. 1A. Cytotoxicity assays demonstrated that treatment with CAG at concentrations up to 50 μM for 24 h and 48 h exhibited no significant cytotoxicity to chondrocytes (Fig. 1B,C). Western blot analysis revealed that TBHP stimulation significantly upregulated the expression of senescence markers p53, CDKN1A, and CDKN2A/p16 (Fig. 1D–G). Notably, CAG pretreatment reversed these changes. Senescence-associated β-galactosidase staining further validated this finding: the proportion of Senescence-associated β-galactosidase (SA-β-gal) positive cells increased in the TBHP group but decreased significantly with CAG treatment (Fig. 1H,I). EdU proliferation assays demonstrated that CAG intervention partially restored TBHP-induced proliferation inhibition (Fig. 1J,K). Additionally, CAG treatment markedly suppressed TBHP-induced upregulation of SASP-associated inflammatory cytokines, including IL-1β (Fig. 1L), IL-6 (Fig. 1M), TNFα (Fig. 1N), IL-17 (Fig. 1O), and matrix-degrading components MMP13 (Fig. 1P). Collectively, these findings indicate that CAG effectively counteracts oxidative stress-mediated chondrocyte senescence and SASP.

CAG ameliorates extracellular matrix metabolic homeostasis

Senescent chondrocytes disrupt ECM homeostasis by suppressing key anabolic components COL2A1 and ACAN while activating catabolic components ADAMTS5 and MMP3, further exacerbated by SASP-driven pro-inflammatory cytokine release[27]. Western blot analysis demonstrated that CAG intervention reversed TBHP-induced downregulation of COL2A1 and ACAN while suppressing ADAMTS5 and MMP3 overexpression (Fig. 2A–E). Immunofluorescence quantification corroborated these results: CAG treatment partially restores COL2A1 fluorescence intensity (Fig. 2F, G)and reduced ADAMTS5 fluorescence intensity (Fig. 2H, I). Alcian

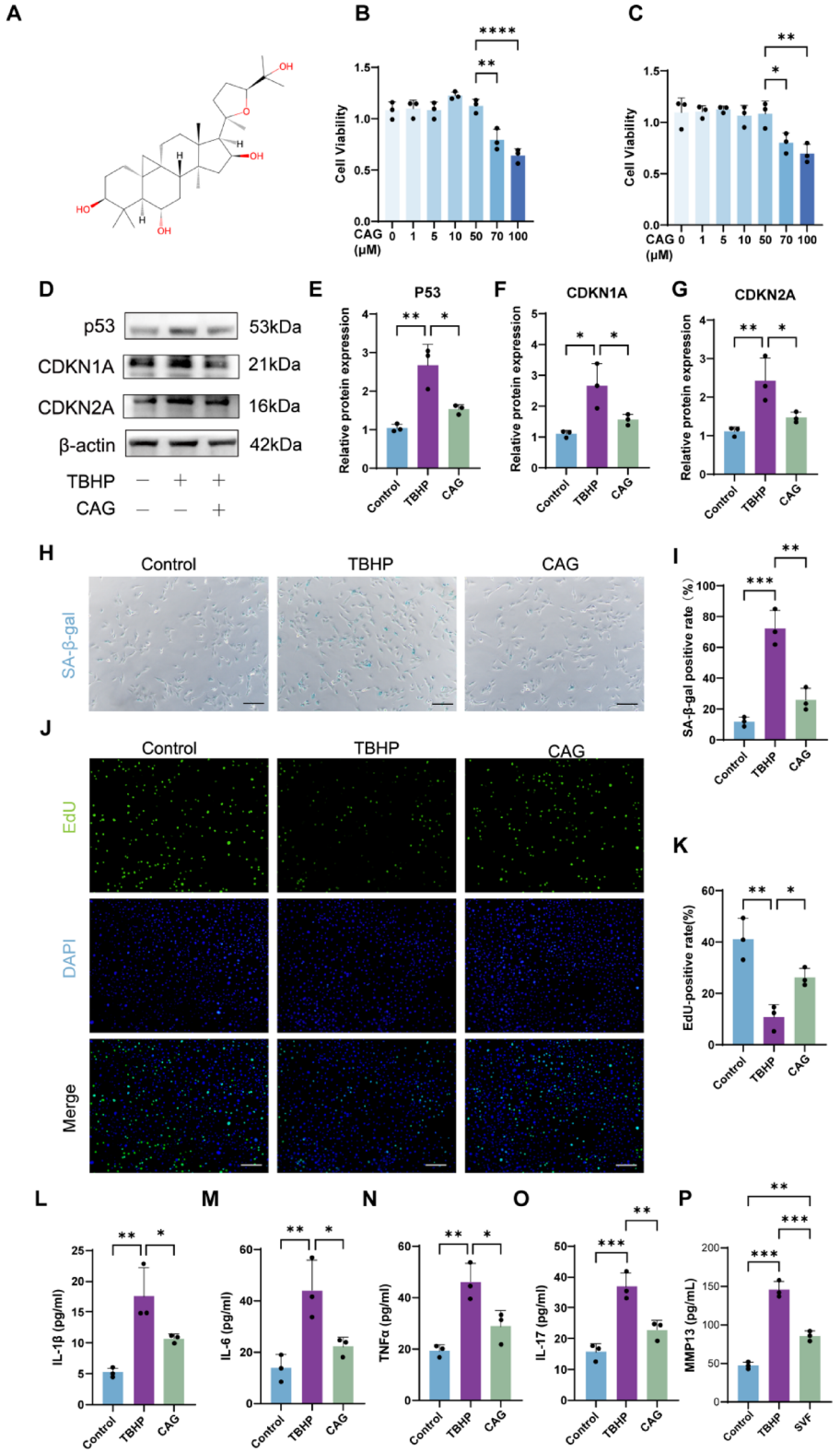

Fig. 1. CAG attenuates oxidative stress-induced chondrocyte senescence. (**A**) Chemical structure of CAG. (**B**) Effects of CAG treatment for 24 h on the viability of chondrocytes were evaluated using the CCK-8 assay. n = 3. (**C**) Effects of CAG treatment for 48 h on the viability of chondrocytes were evaluated using the CCK-8 assay. n = 3. (**D**–**G**) Western blot analysis and quantification of senescence key markers (p53, CDKN1A, CDKN2A) in chondrocytes under CAG (50 μm) and TBHP (50 μm) treatments (See Supplementary Materials for original blots). n = 3. $^{*}p < 0.05$; $^{**}p < 0.01$; $^{***}p < 0.001$. (**H**,**I**) Representative images and quantitative analysis of β-galactosidase staining. n = 3, bar = 50 μm. (**J**,**K**) Representative images and quantitative analysis of EdU staining. n = 3, bar = 50 μm. (**L**–**P**) ELISA quantification of IL-1β, IL-6, TNF-α, IL-17, and MMP13 levels in chondrocytes under different treatments. n = 3. $^{*}p < 0.05$; $^{**}p < 0.01$; $^{***}p < 0.001$.

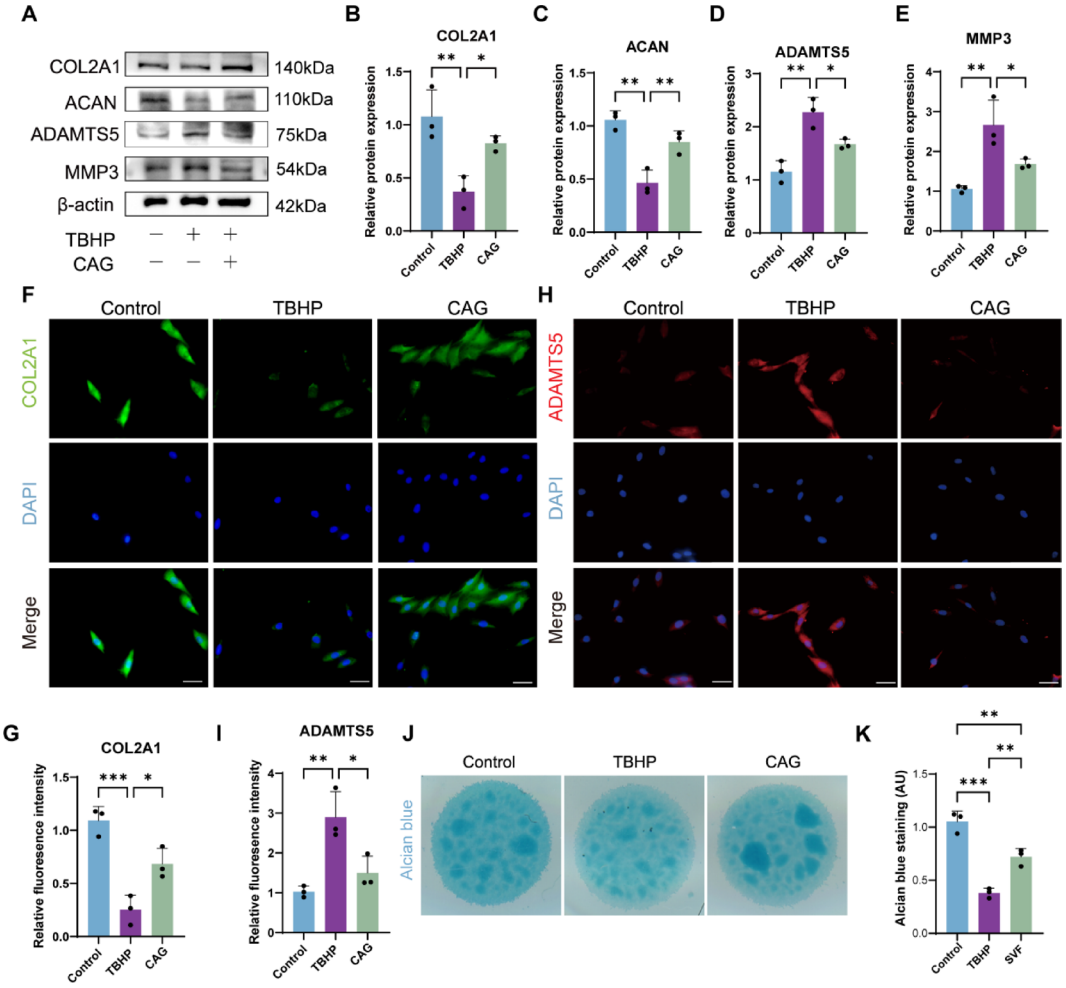

Fig. 2. CAG ameliorates extracellular matrix metabolic homeostasis. (**A**–**E**) Western blot analysis and quantification of extracellular matrix proteins (COL2A1, ACAN, ADAMTS5, MMP3) in chondrocytes under CAG (50 μm) and TBHP (50 μm) treatments (See Supplementary Materials for original blots). n = 3. (**F**,**G**) Representative Immunofluorescence images and quantitative analysis of COL2A1, ADAMTS5. bar = 50 μm. n = 3. (**H**,**I**) Representative Immunofluorescence images and quantitative analysis of ADAMTS5. bar = 50 μm. n = 3.(**J**,**K**) Representative images and quantitative analysis Alcian blue staining of chondrocytes under different treatments. $^{*}p < 0.05$; $^{**}p < 0.01$; $^{***}p < 0.001$.

blue staining confirmed that CAG significantly ameliorated TBHP-induced glycosaminoglycan depletion (Fig. 2J,K), underscoring its protective effects on ECM metabolic imbalance.

CAG mitigates ECM dysfunction and SASP by inhibiting NF-κB pathway

Given the central role of NF-κB in SASP and ECM dysregulation, we elucidated CAG's regulatory effects on this pathway. Here, CAG inhibited TBHP-induced IκBα phosphorylation (p-IκBα) and subsequent degradation, thereby stabilizing cytoplasmic IκBα levels (Fig. 3A–C). Furthermore, CAG suppressed TBHP-triggered p65 phosphorylation and nuclear translocation (Fig. 3D,E). These results systematically demonstrate that CAG mitigates pathological NF-κB activation by stabilizing IκBα and modulating p65 activation status, thereby regulating chondrocyte senescence and ECM homeostasis.

Involvement of NRF2 in CAG-mediated suppression of NF-κB signaling

To explore the mechanisms underlying the anti-senescent effects of CAG, we first examined whether its reported telomerase-activating property contributed to the observed protection[19,22,23]. However, CAG treatment failed to restore telomerase reverse transcriptase (TERT) expression in chondrocytes (Fig. S1), suggesting that its anti-senescent effects are independent of telomerase activation. Previous studies have demonstrated that CAG exerts antioxidant effects in multiple disease models through activation of NRF2, a master regulator of cellular redox homeostasis[28]. Moreover, NRF2 has been shown to play a pivotal role in modulating NF-κB signaling under oxidative stress conditions and in regulating SASP-associated inflammatory responses[29]. Therefore, we examined whether NRF2 participates in the regulatory effects of CAG. Under basal conditions, KEAP1 binds NRF2 and promotes its ubiquitination and proteasomal degradation[30]. To investigate potential interactions, we

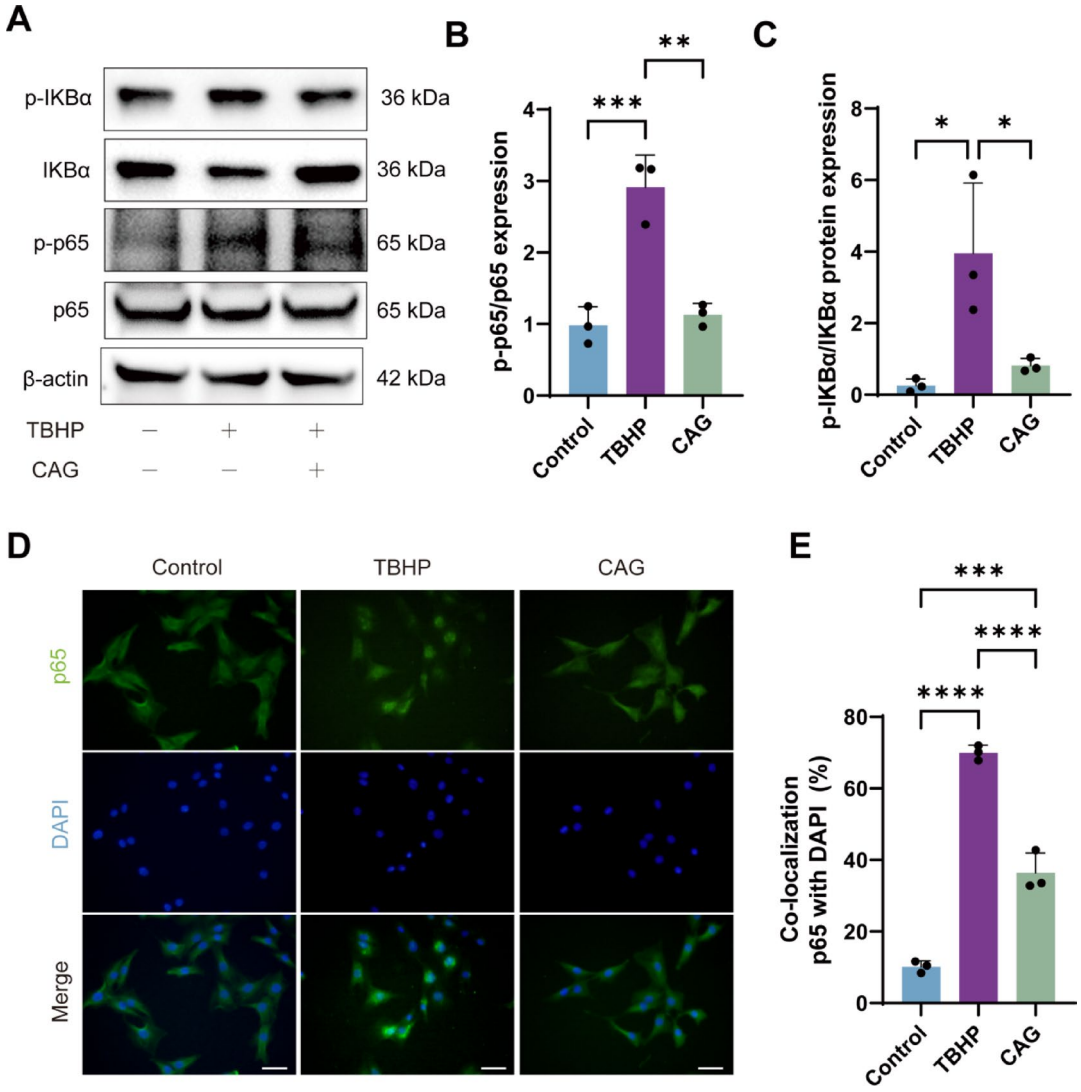

Fig. 3. CAG mitigates ECM dysfunction and SASP by inhibiting NF-κB Pathway. (**A**–**C**) Western blot analysis and quantification of proteins involving NF-κB pathway in chondrocytes under CAG (50μm) and TBHP (50μm) treatments (See Supplementary Materials for original blots). n = 3. (**D**,**E**) Representative immunofluorescence images of p65 protein localization in chondrocytes, bar = 50 μm. n = 3. $^{*}p < 0.05$; $^{**}p < 0.01$; $^{***}p < 0.001$; $^{****}p < 0.0001$.

obtained the chemical structure of CAG from PubChem and predicted the structure of KEAP1 using AlphaFold (Fig. 4A,B). Subsequent molecular docking analysis revealed a binding energy of − 9.1 kcal/mol between CAG and the KEAP1, indicating a strong potential interaction (Fig. 4C). Analysis of the potential binding sites further demonstrated that CAG interacts with multiple residues within the KEAP1 Kelch domain (Fig. 4D). Consistent with the docking results and our hypothesis, western blot analysis showed that CAG treatment was associated with increased protein levels of NRF2 and its downstream targets HO-1, NQO1, and GCLC (Fig. 4E–G). Subcellular fractionation analysis revealed that CAG treatment was accompanied by enhanced NRF2 accumulation in the nuclear fraction under TBHP-induced oxidative stress (Fig. 4I,J). In addition, CAG effectively stabilizes the mitochondrial membrane potential (Fig. 4K,L) and scavenges TBHP-induced ROS (Fig. 4M,N). These results indicate that CAG activates NRF2 signaling in chondrocytes under oxidative stress conditions. The activation of NRF2 signaling was further associated with reduced ROS accumulation and improved mitochondrial membrane potential, supporting a role for NRF2 in mediating the antioxidant effects of CAG.

To assess whether NRF2 is required for the inhibitory effects of CAG on NF-κB signaling, NRF2 expression was silenced using specific siRNAs. Western blot analysis of NRF2 protein expression following transfection with three different NRF2-targeting Small interfering RNA (siRNA) identified siNRF2-1 as the most effective in suppressing NRF2 levels (Fig. 4O,P). Consequently, siNRF2-1 was chosen for use in the following experimental procedures. Notably, knockdown of NRF2 markedly attenuated the protective effects of CAG on mitochondrial membrane potential (Fig. 4Q,R) and intracellular ROS levels under TBHP-induced oxidative stress (Fig. 4S,T). Consistently, inhibition of NRF2 significantly attenuated the suppressive effects of CAG on NF-κB pathway

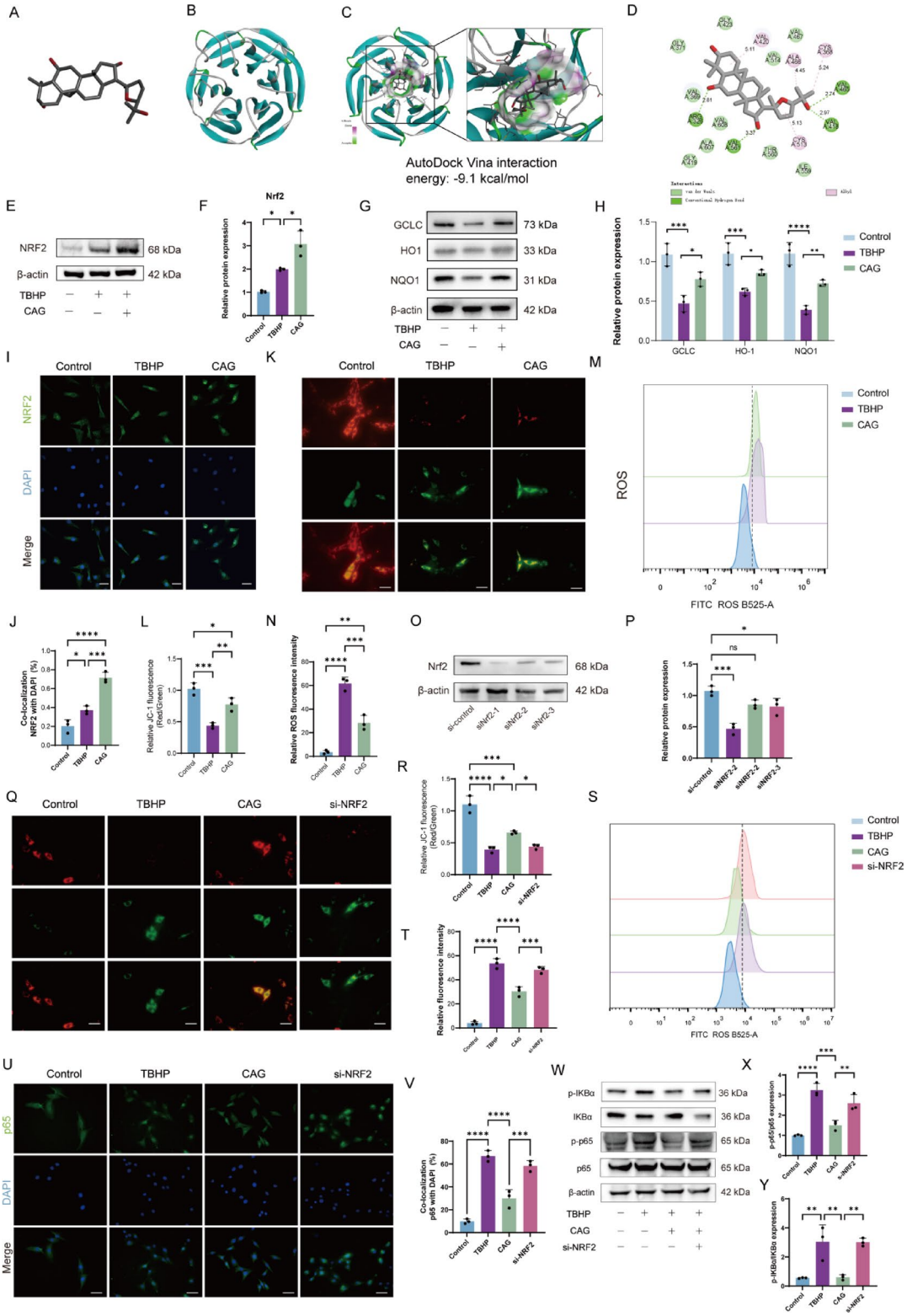

activation. This reversal was evidenced by increased ratios of phosphorylated IκBα to total IκBα (p-IκBα/IκBα) and phosphorylated p65 to total p65 (p-p65/p65) (Fig. 4U,V). Furthermore, immunofluorescence confirmed that NRF2 inhibition partially restored p65 nuclear translocation to levels comparable to those induced by TBHP treatment alone (Fig. 4W–Y). These results indicate that NRF2 is required for CAG-mediated suppression of NF-κB signaling under oxidative stress conditions.

CAG mitigates ECM dysfunction through NRF2 activation

To determine whether NRF2 mediates CAG's regulatory effects on ECM metabolism, we utilized si-NRF2. Protein expression analysis revealed that NRF2 inhibition significantly abolished CAG's effects on key ECM

◀**Fig. 4**. CAG inhibiting NF-κB pathway through NRF2. (**A**) The structure model of CAG. (**B**) The ribbon model of the KEAP1. (**C**) The interaction between CAG and KEAP1; interaction energy is -9.1 kcal/mol. (**D**) The binding model between CAG and KEAP1, and CAG interacts with multiple residues within the KEAP1 Kelch domain. (**E**,**F**) Western blot analysis and quantification of NRF2 protein in chondrocytes under indicated treatments. (**G**,**H**) Western blot analysis and quantification of NRF2 downstream targets HO-1, NQO1, and GCLC proteins. (**I**,**J**) Representative immunofluorescence images and quantification of NRF2 protein localization, bar = 50 μm. n = 3. (**K**,**L**) Immunofluorescence staining and quantification of the effect of CAG on the mitochondrial membrane potential, bar = 50 μm, n = 3. (**M**,**N**) Effects of CAG on ROS levels in chondrocytes measured by flow cytometry. n = 3. (**O**,**P**) Western blot analysis and quantification of NRF2 protein expression in cells transfected with NRF2-targeting siRNAs (siNRF2-1, siNRF2-2, siNRF2-3). (**Q**,**R**) Immunofluorescence staining and quantification of the effect of si-NRF2 on the mitochondrial membrane potential, bar = 50 μm, n = 3. (**S**,**T**) Effects of si-NRF2 on ROS levels in chondrocytes measured by flow cytometry. n = 3. (**U**,**V**) Representative immunofluorescence images of p65 protein localization in chondrocytes under NRF2 inhibition treatment, bar = 50 μm. n = 3. (**W**–**Y**) Western blot analysis and quantification of proteins involving NF-κB pathway in chondrocytes under si-NRF2 transfection treatment (See Supplementary Materials for original blots). n = 3. *$p < 0.05$; **$p < 0.01$; ***$p < 0.001$; ****$p < 0.0001$.

regulators. Specifically, si-NRF2 reversed CAG-induced upregulation of the ECM anabolic components COL2A1 and ACAN, and prevented CAG-mediated downregulation of the catabolic components ADAMTS5 and MMP3 (Fig. 5A–E). Consistent with these findings, Alcian blue staining demonstrated that NRF2 inhibition significantly increased GAG depletion compared to CAG treatment alone (Fig. 5F,G). Furthermore, immunofluorescence analysis confirmed that NRF2 inhibition led to dysregulation of matrix metabolic components, characterized by reduced COL2A1 fluorescence intensity (Fig. 5H,I) and increased ADAMTS5 fluorescence intensity (Fig. 5J,K).

CAG mitigates senescence through NRF2 activation

We subsequently investigate whether NRF2 mediates CAG's regulatory effects on SASP of chondrocytes. Western blot analysis revealed that NRF2 inhibition abolished the inhibitory effects of CAG on key senescence-associated proteins, including p53, CDKN1A, and CDKN2A (Fig. 6A–D). Furthermore, si-NRF2 treatment significantly increased SA-β-gal positive rate compared to CAG treatment alone (Fig. 6E,F). Additionally, EdU staining demonstrated that NRF2 inhibition abrogated the pro-proliferative effect of CAG on chondrocytes (Fig. 6G,H). Collectively, these results demonstrate that CAG suppresses chondrocyte senescence by activating NRF2 signaling.

CAG ameliorates rat OA process in vivo

In a monosodium iodoacetate (MIA)-induced rat osteoarthritis model, intra-articular CAG administration markedly improved joint pathology. Hematoxylin and Eosin (H&E) and Safranin O-Fast Green (S&O) staining revealed that CAG partially restored cartilage thickness, reduced chondrocyte disorganization, and reversed glycosaminoglycan loss (Fig. 7A,B). Osteoarthritis Research Society International (OARSI) and Mankin histological scores significantly decreased in the CAG-treated group compared to the model group (Fig. 7C,D). Immunohistochemical analysis demonstrated that CAG treatment rescued COL2A1 expression while suppressing ADAMTS5 expression. Additionally, CAG reduced p21-positive senescent cells and enhanced NRF2 positive rate, confirming its role in ameliorating ECM metabolic imbalance and cellular senescence via NRF2 pathway activation (Fig. 7E–I).

Discussion

Osteoarthritis, a multifactorial disease characterized by degenerative changes in articular cartilage, manifests pathologically as ECM metabolic imbalance, aberrant inflammation, and oxidative stress, ultimately leading to joint structural destruction and functional impairment[6,31]. Current therapeutic strategies primarily alleviate symptoms but fail to halt disease progression[4,5]. While a variety of cell-based therapeutic strategies have been explored for osteoarthritis treatment, including mesenchymal stem/stromal cell (MSC)[32], and stromal vascular fraction (SVF)[33] have demonstrated promising therapeutic efficacy in OA treatment, their requirement for invasive procedures introduces significant risks compared to minimally invasive approaches like local drug injection[34,35]. Consequently, there is a compelling clinical need to explore alternative therapeutic agents that circumvent the limitations of cell-based therapies. Recent advances in OA pathogenesis research have further highlighted the central role of cellular senescence and oxidative stress in disease development and progression. Chondrocyte senescence is a key driver accelerating joint degeneration, while excessive generation of ROS exacerbates inflammatory cascades and ECM degradation[10,31]. Therefore, targeting these fundamental mechanisms through anti-senescence and antioxidant strategies represents a highly promising therapeutic rationale for not only alleviating symptoms but also potentially modifying OA progression. The development of such agents could provide viable and safer alternatives to cell-based therapies like SVF.

CAG, one of the known natural compound capable of activating human telomerase, offers a novel therapeutic approach for OA due to its unique anti-aging and antioxidant properties[19,22,23]. Our study demonstrates that CAG counteracts oxidative stress-induced ECM dysregulation and SASP in chondrocytes, potentially via modulation of the NRF2/NF-κB pathway. In vivo experiments further confirm that CAG treatment mitigates OA progression in a rat model.

Oxidative stress disrupts joint microenvironment homeostasis through multiple mechanisms, with chondrocyte senescence and ECM metabolic dysregulation serving as critical pathological hallmarks[12]. Studies

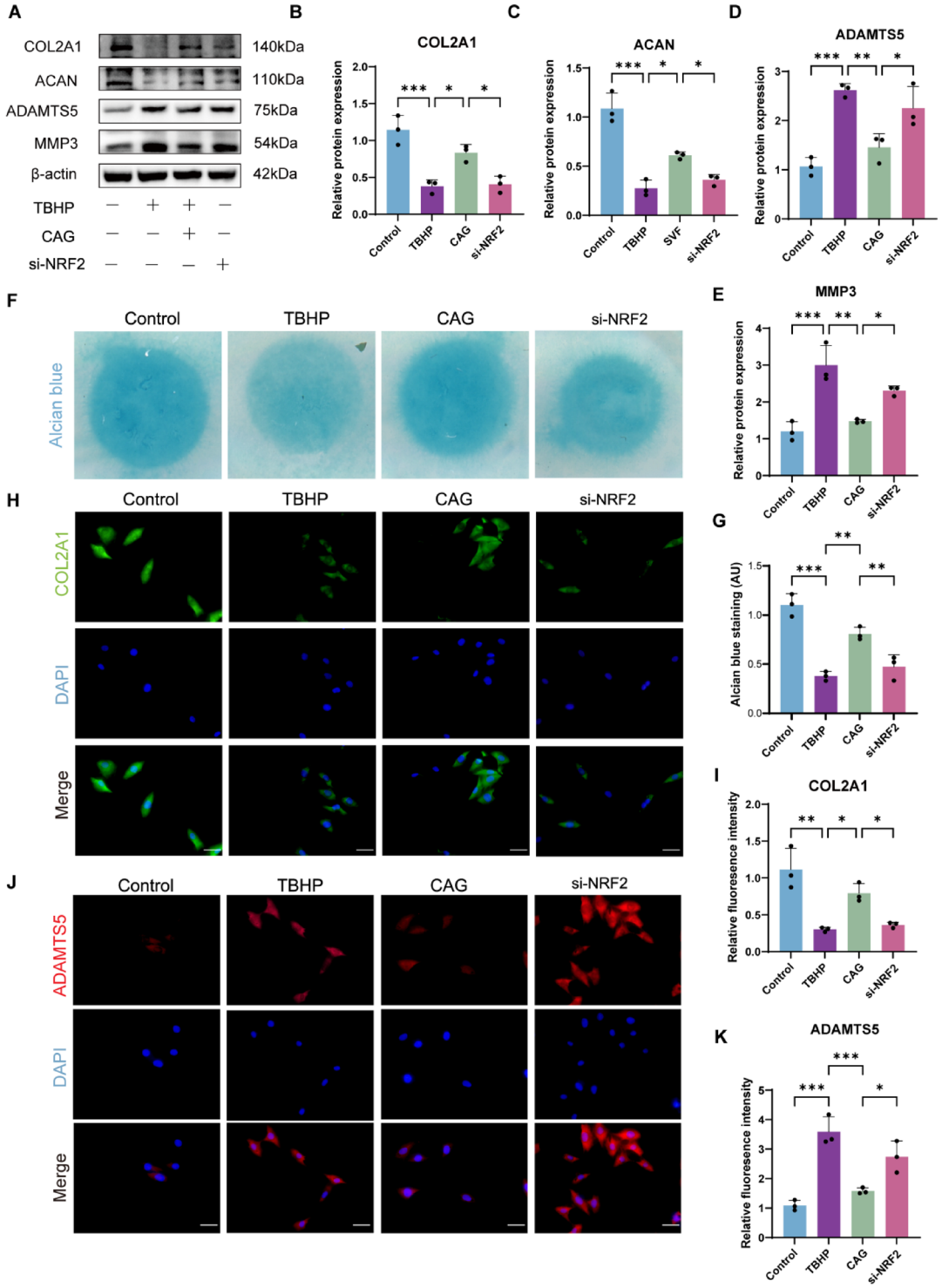

Fig. 5. CAG mitigates ECM dysfunction through NRF2 activation. (**A**–**E**) Western blot analysis and quantification of extracellular matrix proteins (COL2A1, ACAN, ADAMTS5, MMP3) in chondrocytes under NRF2 inhibition treatment (See Supplementary Materials for original blots). n = 3. (**F**,**G**) Representative images and quantitative analysis alcian blue staining of chondrocytes under si-NRF2 transfection treatment. (**H**,**I**) Representative immunofluorescence images and quantitative analysis of COL2A1. n = 3. (**J**,**K**) Representative immunofluorescence images and quantitative analysis of ADAMTS5. n = 3. $^{*}p < 0.05$; $^{**}p < 0.01$; $^{***}p < 0.001$; $^{****}p < 0.0001$.

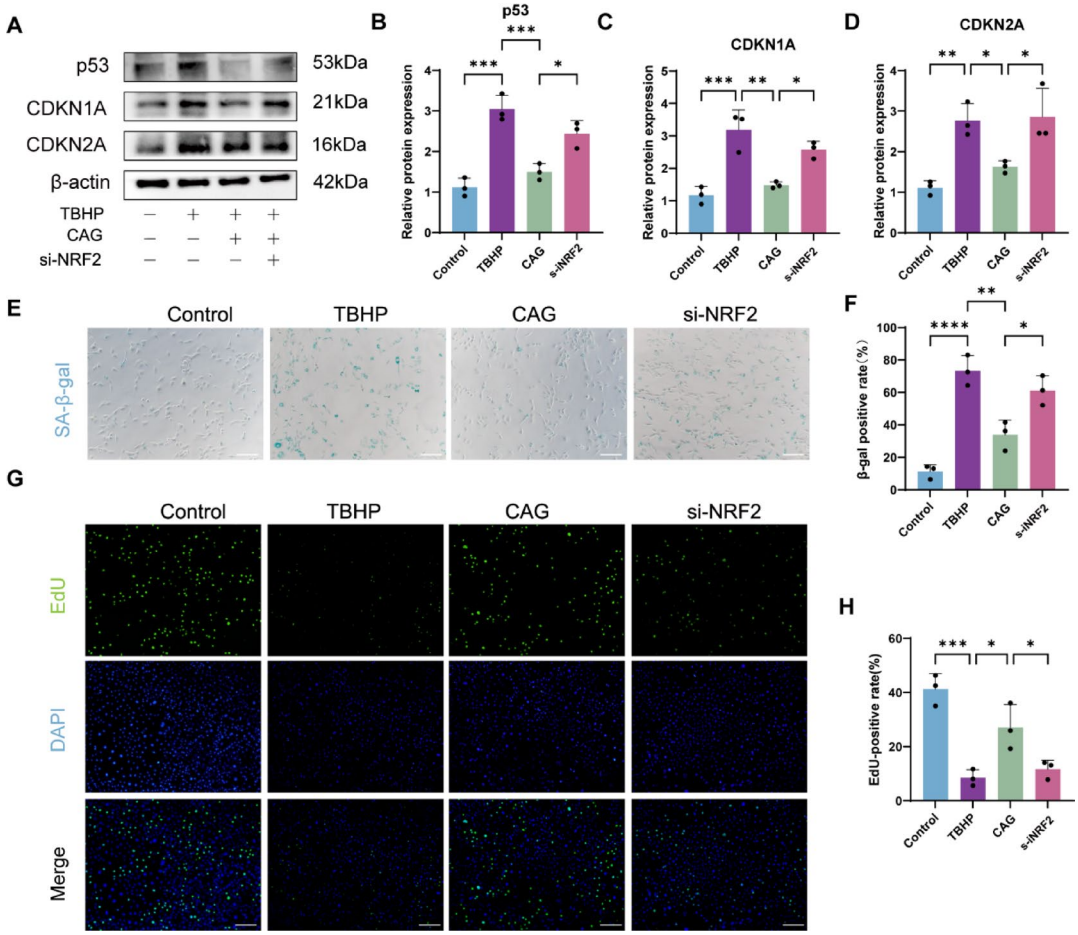

Fig. 6. CAG mitigates senescence through NRF2 activation. (**A**–**D**) Western blot analysis and quantification of senescence key markers (p53, CDKN1A, CDKN2A) in chondrocytes under si-NRF2 transfection treatments (See Supplementary Materials for original blots). n = 3. (**E**,**F**) Representative images and quantitative analysis of β-galactosidase staining. n = 3, bar = 50 μm. (**G**,**H**) Representative images and quantitative analysis of EdU staining. n = 3, bar = 50 μm. $^{*}p < 0.05$; $^{**}p < 0.01$; $^{***}p < 0.001$; $^{****}p < 0.0001$.

indicate that oxidative stress directly impairs mitochondrial function in chondrocytes, creating a self-reinforcing cycle of ROS overproduction that precipitates premature senescence[36]. Senescent cells, via SASP, release pro-inflammatory cytokines and matrix-degrading proteins, which amplify local inflammation and disrupt ECM homeostasis by suppressing collagen II and aggrecan synthesis while upregulating catabolic components such as MMP3 and ADAMTS5[10]. In this study, CAG significantly attenuated oxidative stress-induced chondrocyte senescence and reduced levels of IL-1β, TNFα, and IL-6. Furthermore, CAG partially restored ECM metabolic balance by inhibiting ADAMTS5 and MMP3 expression while enhancing COL2A1 and aggrecan production. In vivo findings corroborated these effects, with CAG reversing cartilage matrix destruction and cellular senescence, underscoring its therapeutic potential for OA.

The NF-κB pathway, a key transcriptional regulator of inflammatory responses and SASP-related cytokine production, exists in an inactive cytoplasmic complex with its inhibitor IκB under physiological conditions[37]. Oxidative stress triggers IκB phosphorylation and degradation, liberating NF-κB to translocate into the nucleus and drive pro-inflammatory gene levels[38,39]. Our data demonstrate that CAG treatment effectively suppressed oxidative stress-induced IκB degradation and p65 phosphorylation, thereby inhibiting NF-κB pathway activation. This dual inhibition positions CAG as a potent modulator of both inflammatory and senescence-related pathways in OA.

To elucidate how CAG inhibits NF-κB activation under oxidative stress, we focused on NRF2, the master regulator of cellular antioxidant responses[14]. Under basal conditions, KEAP1 facilitates NRF2 ubiquitination and proteasomal degradation. Oxidative stress disrupts KEAP1-NRF2 binding, enabling NRF2 nuclear translocation and transcriptional activation of antioxidant genes[40]. Prior studies suggest that NRF2 activation suppresses signaling, offering therapeutic benefits in OA[41,42]. As a primary bioactive component of Astragalus membranaceus—a traditional herb with established NRF2-activating properties—CAG was hypothesized to exert similar effects[22,23]. Molecular docking analysis suggested a potential interaction between CAG and the Kelch domain of KEAP1, which may be involved in the regulation of NRF2 signaling. Consistent with this, CAG markedly upregulated NRF2 expression in chondrocytes. Independently, we observed that CAG treatment

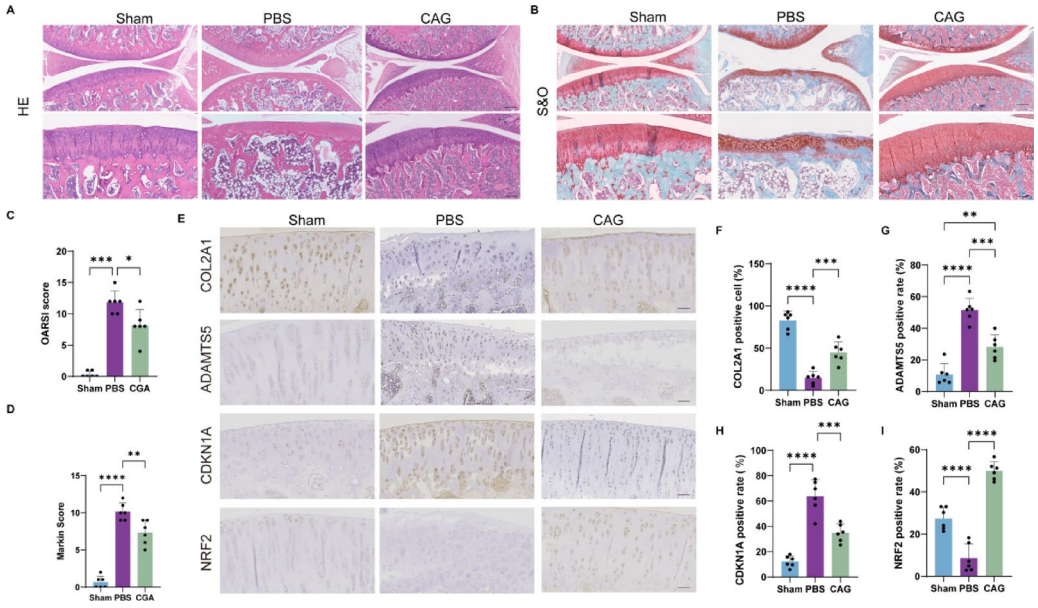

Fig. 7. CAG ameliorates rat OA process in vivo. (**A**) Representative images of hematoxylin and eosin (H&E) staining showing changes in articular cartilage at 4 weeks post-treatment. Upper bar = 500 μm, lower bar = 200 μm. (**B**) Representative images of Safranin O/Fast Green (S&O) staining showing changes in articular cartilage. Upper bar = 500 μm, lower bar = 200 μm. (**C**,**D**) Quantification of articular cartilage degeneration using the OARSI and Mankin scoring systems. n = 6. (**E**–**I**) Representative images and quantitative analysis of COL2A1-, ADAMTS5-, p21-, and NRF2-positive cells in articular cartilage at 4 weeks post-surgery. n = 6, bar = 200 μm. *$p < 0.05$; **$p < 0.01$; ***$p < 0.001$; ****$p < 0.0001$.

was associated with increased NRF2 protein levels in chondrocytes. Importantly, genetic silencing of NRF2 abrogated the inhibitory effects of CAG on NF-κB signaling, SASP-associated inflammatory factors, and matrix-metabolizing proteins, indicating that NRF2 is required for the chondroprotective actions of CAG.

There are several limitations in our study. First, although NRF2 knockdown attenuated the inhibitory effects of CAG on NF-κB activation, we cannot exclude the involvement of parallel or reciprocal regulatory mechanisms between these pathways. Definitive establishment of pathway hierarchy will require gain-of-function and rescue approaches. Second, While NRF2 mediated the biological effects of CAG, they do not establish a direct molecular interaction or define the precise mechanistic sequence linking KEAP1 binding, NRF2 stabilization, and downstream transcriptional activity. Future investigations incorporating these approaches will be essential to delineate the directness and specificity of the proposed CAG–KEAP1–NRF2 regulatory mechanism. Third, we employed TBHP-induced oxidative stress as an in vitro model to investigate chondrocyte senescence and extracellular matrix dysregulation. While this approach effectively mimics redox imbalance–driven cellular dysfunction, it does not fully capture the complex inflammatory microenvironment of osteoarthritic joints. Inflammatory cytokines such as IL-1β are well-established mediators of cartilage degeneration and represent an important complementary model. Future studies incorporating IL-1β stimulation or combined oxidative–inflammatory paradigms will be required to further validate the translational relevance of CAG in osteoarthritis.

Materials and methods

Isolation and culture of primary chondrocytes

Primary chondrocytes were isolated from the articular cartilage of knee joints harvested from 6-week-old male Sprague–Dawley (SD) rats[43]. The rats were purchased from Phenotek Bio Technology (Shanghai, China). Knee joints underwent surface disinfection followed by extensive rinsing in sterile phosphate-buffered saline (PBS). Cartilage tissues were then minced and subjected to enzymatic digestion using 0.2% type II collagenase for approximately 6 h at 37 °C. Chondrocytes were subsequently recovered. Following isolation, the cells were resuspended in high-glucose DMEM enriched with 10% fetal bovine serum (abs972, Absin Bioscience) and maintained at 37 °C in a humidified atmosphere containing 5% CO_2. Cells were detached for subculture using a 0.25% trypsin–EDTA solution when cultures attained approximately 80% confluence. For all downstream experiments, only passage 2 chondrocytes in their logarithmic phase of growth were utilized. For drug treatment, CAG (MCE, HY-N1485) was added to the culture system for 24 h. Subsequently, *tert*-butyl hydroperoxide (TBHP, 50 μM; B106035, Aladdin) was supplemented into the medium a for an additional 24 h of treatment.

Small interfering RNA transfection

Targeting siRNA against the NRF2 gene (si-NRF2) and negative control siRNA (si-Con) were synthesized by GeneCreate Biological Engineering Co., Ltd (Wuhan, China). Chondrocytes were transfected using Lipofectamine 3000 (Thermo Fisher, USA) when they reached 70–80% confluence. siRNA solutions were

prepared by diluting si-NRF2 or si-Con to a final concentration of 20 nM in 250 μL of serum-free Opti-MEM medium, followed by gentle mixing and incubation at room temperature for 5 min. The diluted siRNA was then combined with the diluted Lipofectamine 3000 reagent, mixed gently, and incubated at room temperature for 15 min to allow complex formation. The resulting siRNA-Lipofectamine 3000 complexes were added to the cells. Cells were harvested 48 h post-transfection for subsequent experiments.

Cell viability assay

Cellular activity was quantified with the Cell Counting Kit-8 (CCK8, 40203ES60, Yeasen) following standardized protocols. Chondrocytes were plated at a density of $\sim 5 \times 10^3$ cells/well within 96-well microplates. After exposure to incremental CAG concentrations, media was replaced with CCK-8 working solution diluted 1:10 in fresh culture medium. Following 1 h incubation at 37 °C under light-protected conditions, spectrophotometric quantification of formazan dye conversion was performed at 450 nm a microplate reader (BioTek Synergy H1, USA).

Western blot

Total cellular protein was isolated with RIPA lysis buffer (P0013B, Beyotime) containing protease and phosphatase inhibitors. Protein quantification was performed using a commercially available BCA assay kit (P0009, Beyotime) according to standardized protocols. Equal amounts of protein were separated by SDS-PAGE and subsequently transferred onto PVDF membranes (IPVH304F0, Merck). After blocking with 10% BSA (B885114, Macklin) for 1 h at room temperature, membranes were incubated with primary antibodies overnight at 4 °C, followed by appropriate HRP-conjugated secondary antibodies. Protein bands were visualized using ECL chemiluminescent substrate and imaged with a Syngene G:BOX ChemiXT4 system (Syngene, UK).

Primary antibodies against COL2A1 (1:1000, YT1022, Immunoway), ADAMTS5 (1:1000, A2836, ABclonal), Aggrecan (1:500, A11691, ABclonal), MMP3 (1:1000, A1202, ABclonal), CDKN2A (1:1000, ab51243, Abcam), p53 (1:1000, ab32049, Abcam), CDKN1A (1:1000, ab109520, Abcam), NRF2 (1:1000, A3577, ABclonal), IKBα (1:1000, A19714, ABclonal), p-IKBα (1:1000, AP0707, ABclonal), p65 (1:1000, A19653 ABclonal), p-p65 (1:1000, AP1294, ABclonal), HO-1(1:5000, A28140PM, ABclonal), NQO1 (1:1000, A19586, ABclonal), GCLC (1:1000, A4499, ABclonal), Histone H3 (1:1000, A2348, ABclonal), and β-actin (1:1000, AC006, ABclonal) were used.

Intracellular ROS detection

Intracellular ROS levels were measured using the fluorescent probe 2′,7′-dichlorodihydrofluorescein diacetate (DCFH-DA, S1105S, Beyotime). Briefly, chondrocytes were treated as indicated, washed with PBS, and incubated with 10 μM DCFH-DA at 37 °C for 30 min in the dark. After washing, fluorescence intensity was documented using flow cytometry (Beckman CytoFlexS) and quantified using FlowJo™ software (v10.0.0; BD Biosciences), with fluorescence intensity normalized to untreated controls.

Mitochondrial membrane potential detection

The mitochondrial membrane potential was assessed using a JC-1 assay kit (M8650, Solarbio). Briefly, rat chondrocytes were incubated with 5 μM JC-1 staining solution for 20 min at 37 °C in the dark. After washing, the cells were immediately imaged using a fluorescence microscope (IX73, Olympus, Tokyo, Japan). The fluorescence intensity of JC-1 aggregates and monomers was quantified using ImageJ software (NIH, USA). The mitochondrial membrane potential level was represented by the red/green fluorescence intensity ratio, with a decreased ratio indicating mitochondrial depolarization.

Immunofluorescence

Following treatment, chondrocytes underwent fixation in 4% paraformaldehyde, permeabilization with 0.1% Triton X-100 for 10 min, and blocking with 5% BSA for 1 h. Primary antibodies COL2A1 (1:100, YT1022, Immunoway), ADAMTS5 (1:200, A2836, ABclonal) , p65 (1:200, A19653 ABclonal), were incubated overnight at 4 °C. After PBS washes, cells were incubated with Alexa Fluor 488- or 594-conjugated secondary antibodies (ZF-0511, ZF-0516, ZSGB-bio) for 1 h at room temperature. Nuclei were counterstained with DAPI (40728ES03, Yeasen) for 5 min. Images were captured using a fluorescence microscope (Olympus IX73). For each sample, at least five randomly selected fields were imaged at the same magnification. Mean fluorescence intensities were quantified in ImageJ (NIH) and normalized to untreated controls.

Alcian blue staining

Alcian blue staining was performed in 48-well plates. Post-treatment, cells were fixed with 4% paraformaldehyde (15 min, room temperature). The cells were then pretreated with Alcian blue acidification solution (75881-23-1, Solarbio) for 3 min, followed by staining with Alcian blue solution (pH 2.5) for 30 min at room temperature. Finally, cells were washed three times with PBS and imaged under a light microscope. For glycosaminoglycan quantification, bound dye was extracted using guanidine hydrochloride, and the absorbance of the extracted dye was measured at 620 nm using a spectrophotometer. All measurements were performed using the *entire well area* under identical conditions[44].

SA-β-gal staining

Cellular senescence was evaluated using a commercial senescence detection kit (G1580, Solarbio). Post-fixation specimens were subjected to chromogenic incubation with the staining working solution (pH 6.0) at 37 °C without CO_2 overnight. Following PBS washes, stained cells were imaged under bright-field microscopy.

EdU staining

Following treatment, cells were incubated with 10 μM EdU working solution (0071L, Beyotime) in DMEM medium for 2 h at 37 °C. After fixation with 4% paraformaldehyde and permeabilization with 0.5% Triton X-100, the Click reaction cocktail was added and incubated for 30 min. Nuclei were counterstained with Hoechst 33342. Fluorescent images were captured using a fluorescence microscope.

ELISA assay

Levels of SASP-associated inflammatory and matrix-degrading components (IL-1β, IL-6, IL-17, TNF-α, MMP13) were quantified using commercial ELISA kits (IL-1β: E-EL-R0012; IL-6: E-EL-R0015; IL-17: E-EL-R0566; TNF-α: E-EL-R2856; MMP13: E-EL-R0045 all from Elabscience Biotechnology) according to the manufacturers' instructions. Briefly, Cell culture supernatants were collected after the indicated treatments and centrifuged at 1000×*g* for 10 min at 4 °C to remove cell debris. The clarified supernatants were then transferred to pre-coated microplate wells for ELISA analysis.

For intracellular TERT measurement, cells were harvested after treatment and lysed using the extraction buffer provided with the ELISA kit (JLC-Y2180, Gelatins) according to the manufacturer's protocol. The lysates were centrifuged to remove insoluble debris, and the resulting supernatants were used for TERT ELISA analysis.

After incubation, detection antibody working solution was added to each well and incubated for 1 h at 37 °C. Plates were washed, followed by the addition of HRP-conjugate working solution. After further incubation and washing, 3,3′,5,5′-Tetramethylbenzidine (TMB) substrate solution was added and allowed to develop in the dark for 30 min. The enzymatic reaction was stopped by adding stop solution. Absorbance was immediately measured at 450 nm.

Histological analysis

Following fixation and decalcification, rat knee joint specimens were embedded in paraffin and sectioned at a thickness of 4 μm. Deparaffinized sections were stained with H&E to assess overall tissue morphology. S&O staining was employed to evaluate proteoglycan content within the cartilage matrix. The severity of cartilage degeneration was independently scored by two blinded observers using the OARSI grading system and the Mankin scoring system.

Immunohistochemistry

Deparaffinized and rehydrated paraffin-embedded sections underwent antigen retrieval using pepsin digestion solution. Endogenous peroxidase activity was quenched by incubation with 3% hydrogen peroxide. Non-specific binding sites were blocked with 10% normal goat serum. Sections were then incubated overnight at 4 °C with the following primary antibodies: COL2A1 (1:100, YT1022, Immunoway), ADAMTS5 (1:200, A2836, ABclonal), CDKN1A (1:1000, ab109520, Abcam), and NRF2 (1:1000, A3577, ABclonal). After washing, sections were incubated for 1 h at room temperature with horseradish peroxidase (HRP)-conjugated goat anti-rabbit (or appropriate species) secondary antibodies. Color development was performed using 3,3′-diaminobenzidine (DAB; DA1010, Solarbio), followed by counterstaining with hematoxylin (C0107, Beyotime). For quantitative analysis, the percentage of positively stained chondrocytes within the articular cartilage was calculated for each section using the formula: (Number of DAB-positive chondrocytes / Total number of chondrocytes in the region of interest) × 100%. The NRF2 positive rate was defined as the percentage of NRF2-positive nuclei relative to the total number of hematoxylin-counterstained nuclei. All analyses were performed independently by two blinded investigators using ImageJ software.

Molecular docking

To investigate potential interactions, semi-flexible docking was performed to generate stable complexes. The structure of CAG; (PubChem CID: 13943286) was downloaded from the PubChem database (https://pubchem.ncbi.nlm.nih.gov/). Its 3D structure was constructed and energy-minimized using ChemDraw 20.0. The protein structure of KEAP1 (UniProt ID: Q14145) was obtained from the AlphaFold Protein Structure Database (https://alphafold.ebi.ac.uk/; model AF-Q14145-F1). Protein preparation, including the removal of water molecules and extraneous ligands, followed by the addition of hydrogen atoms, was conducted using PyMOL 2.4. Docking simulations were carried out using AutoDock Vina 1.1.2. The search space encompassed the entire protein structure to allow for unbiased binding site identification. The simulation was configured to output the 10 best docking poses ranked by predicted binding affinity. The most probable binding mode was selected based on the conformation exhibiting the lowest binding energy and the highest cluster population frequency. To ensure reproducibility, the docking procedure was repeated three times independently; the reported binding energy represents the mean value ± standard deviation of these replicates. Finally, visualization and analysis of the docking results, including protein–ligand interactions, were performed using PyMOL 2.4 and Discovery Studio Visualizer 2019.

In vivo experiments

Animal experiments were approved by the Institutional Animal Care and Use Committee (IACUC) of Western Biomedical (Approval No. 20231218S0501231[02]) and conducted in accordance with the 3R principles. Eighteen 6-week-old male SD rats were purchased from Phenotek Bio Technology (Shanghai, China)[45,46]. All animal experiments were conducted following ARRIVE 2.0 guidelines. All animals were randomly assigned to groups using a computer-generated random number sequence. Osteoarthritis model was induced in the knee joints via intra-articular injection of MIA (HY-D0849, MCE)[47]. Briefly, rats were anesthetized by intraperitoneal injection of sodium pentobarbital. A single injection of MIA in a volume of 2.5 mg was administered into the intra-articular space of the right knee joint using a 29-gauge needle. One week after MIA injection, rats received

weekly intra-articular injections of either phosphate-buffered saline (PBS group) or cycloastragenol (CAG group) at a volume of 50 μL per joint. CAG was administered at a concentration of 50 μM, which was determined based on our preliminary in vitro dose–response experiments. Four weeks after the initial MIA injection, rats were euthanized by overdose of sodium pentobarbital following deep anesthesia, and knee joint tissues were harvested for subsequent analysis.

Statistical analysis

In this study, the data were derived from at least three independent experiments, with all the results expressed as means ± standard deviations (SDs). All experiments were performed in at least three independent biological replicates. The number of independent replicates for each specific experiment is denoted as n and is indicated in the corresponding figure legends. Comparisons between two groups were performed using unpaired t tests, whereas comparisons among multiple groups were conducted using one-way analysis of variance (ANOVA) followed by Tukey's test. Histological scores were analyzed using the Kruskal–Wallis test, followed by Dunn's multiple comparisons test. Statistical analyses were carried out using GraphPad Prism software (Version 9.0, GraphPad Software, San Diego, CA). Differences were considered statistically significant at $p < 0.05$.

Conclusion

This study delineates a mechanistic association between CAG treatment and the attenuation of oxidative stress–induced inflammatory signaling in osteoarthritic chondrocytes. Our data demonstrate that CAG enhances NRF2-mediated antioxidant responses and is accompanied by reduced NF-κB pathway activation, thereby alleviating chondrocyte senescence, SASP propagation, and ECM degradation. These findings highlight the therapeutic potential of CAG in osteoarthritis. Future investigations into dose optimization, long-term efficacy, and combinatorial therapies with existing treatments will further validate its clinical translatability.

Data availability

The datasets used in the current study are available from the corresponding author on reasonable request.

Received: 10 October 2025; Accepted: 28 February 2026
Published online: 12 March 2026

References

1. GBD 2021 Osteoarthritis Collaborators. Global, regional, and national burden of osteoarthritis, 1990-2020 and projections to 2050: A systematic analysis for the Global Burden of Disease Study 2021. *Lancet. Rheumatol.* **5**, e508–e522. https://doi.org/10.1016/S2665-9913(23)00163-7 (2023).
2. Cieza, A. et al. Global estimates of the need for rehabilitation based on the global burden of disease study 2019: A systematic analysis for the global burden of disease study 2019. *Lancet* **396**, 2006–2017. https://doi.org/10.1016/S0140-6736(20)32340-0 (2021).
3. Dieleman, J. L. et al. US spending on personal health care and public health, 1996-2013. *JAMA* **316**, 2627–2646. https://doi.org/10.1001/jama.2016.16885 (2016).
4. Katz, J. N., Arant, K. R. & Loeser, R. F. Diagnosis and treatment of hip and knee osteoarthritis: A review. *JAMA* **325**, 568–578. https://doi.org/10.1001/jama.2020.22171 (2021).
5. Hunter, D. J. & Bierma-Zeinstra, S. Osteoarthritis. *Lancet* **393**, 1745–1759. https://doi.org/10.1016/S0140-6736(19)30417-9 (2019).
6. Rahmati, M., Nalesso, G., Mobasheri, A. & Mozafari, M. Aging and osteoarthritis: Central role of the extracellular matrix. *Ageing Res. Rev.* **40**, 20–30. https://doi.org/10.1016/j.arr.2017.07.004 (2017).
7. Ansari, M. Y., Ahmad, N. & Haqqi, T. M. Oxidative stress and inflammation in osteoarthritis pathogenesis: Role of polyphenols. *Biomed. Pharmacother.* **129**, 110452. https://doi.org/10.1016/j.biopha.2020.110452 (2020).
8. Loeser, R. F., Collins, J. A. & Diekman, B. O. Ageing and the pathogenesis of osteoarthritis. *Nat. Rev. Rheumatol.* **12**, 412–420. https://doi.org/10.1038/nrrheum.2016.65 (2016).
9. Mehana, E.-S.E., Khafaga, A. F. & El-Blehi, S. S. The role of matrix metalloproteinases in osteoarthritis pathogenesis: An updated review. *Life Sci.* **234**, 116786. https://doi.org/10.1016/j.lfs.2019.116786 (2019).
10. Jeon, O. H. et al. Local clearance of senescent cells attenuates the development of post-traumatic osteoarthritis and creates a pro-regenerative environment. *Nat. Med.* **23**, 775–781. https://doi.org/10.1038/nm.4324 (2017).
11. Kang, D. et al. Stress-activated miR-204 governs senescent phenotypes of chondrocytes to promote osteoarthritis development. *Sci. Transl. Med.* https://doi.org/10.1126/scitranslmed.aar6659 (2019).
12. Coryell, P. R., Diekman, B. O. & Loeser, R. F. Mechanisms and therapeutic implications of cellular senescence in osteoarthritis. *Nat. Rev. Rheumatol.* **17**, 47–57. https://doi.org/10.1038/s41584-020-00533-7 (2021).
13. Di Micco, R., Krizhanovsky, V., Baker, D. & d'Adda di Fagagna, F. Cellular senescence in ageing: From mechanisms to therapeutic opportunities. *Nat. Rev. Mol. Cell Biol.* **22**, 75–95. https://doi.org/10.1038/s41580-020-00314-w (2021).
14. Liu, S., Pi, J. & Zhang, Q. Signal amplification in the KEAP1-NRF2-ARE antioxidant response pathway. *Redox Biol.* **54**, 102389. https://doi.org/10.1016/j.redox.2022.102389 (2022).
15. Lo, S. C., Li, X., Henzl, M. T., Beamer, L. J. & Hannink, M. Structure of the Keap1:Nrf2 interface provides mechanistic insight into Nrf2 signaling. *EMBO J.* **25**, 3605–3617. https://doi.org/10.1038/sj.emboj.7601243 (2006).
16. Zhou, S., Liao, F. & Wen, H. Isoquercetin alleviates osteoarthritis via regulating the NOX4/Nrf2 redox imbalance in senescent chondrocytes. *Int. J. Biol. Macromol.* **306**, 141562. https://doi.org/10.1016/j.ijbiomac.2025.141562 (2025).
17. Jiang, C. et al. Therapeutic effect of edaravone on osteoarthritis: Targeting NRF2 signaling and mitochondrial function. *J. Orthop. Translat.* **52**, 220–232. https://doi.org/10.1016/j.jot.2025.04.008 (2025).
18. Wu, J. et al. Cycloastragenol protects against glucocorticoid-induced osteogenic differentiation inhibition by activating telomerase. *Phytother. Res.* **35**, 2034–2044. https://doi.org/10.1002/ptr.6946 (2021).
19. Chen, G. et al. Cycloastragenol reduces inflammation in CLP-induced septic mice by suppressing TLR4 signaling pathways. *Phytomedicine* **142**, 156645. https://doi.org/10.1016/j.phymed.2025.156645 (2025).
20. Hong, H. et al. Cycloastragenol and Astragaloside IV activate telomerase and protect nucleus pulposus cells against high glucose-induced senescence and apoptosis. *Exp. Ther. Med.* **22**, 1326. https://doi.org/10.3892/etm.2021.10761 (2021).
21. Tsoukalas, D. et al. Discovery of potent telomerase activators: Unfolding new therapeutic and anti-aging perspectives. *Mol. Med. Rep.* **20**, 3701–3708. https://doi.org/10.3892/mmr.2019.10614 (2019).

22. Li, Y. et al. Astragaloside IV and cycloastragenol promote liver regeneration through regulation of hepatic oxidative homeostasis and glucose/lipid metabolism. *Phytomedicine* **135**, 156165. https://doi.org/10.1016/j.phymed.2024.156165 (2024).
23. Feng, L. et al. Cycloastragenol reduces microglial NLRP3 inflammasome activation in Parkinson's disease models by promoting autophagy and reducing Scrib-driven ROS. *Phytomedicine* **135**, 156210. https://doi.org/10.1016/j.phymed.2024.156210 (2024).
24. Kang, D. et al. Selenophosphate synthetase 1 deficiency exacerbates osteoarthritis by dysregulating redox homeostasis. *Nat. Commun.* **13**, 779. https://doi.org/10.1038/s41467-022-28385-7 (2022).
25. Shiyuan, L., Biao, W., Xinjia, H. & Huading, L. Sirtuin 4 (Sirt4) downregulation contributes to chondrocyte senescence and osteoarthritis via mediating mitochondrial dysfunction. *Int. J. Biol. Sci.* https://doi.org/10.7150/ijbs.85585 (2024).
26. Xu, X. X. et al. Theaflavin protects chondrocytes against apoptosis and senescence via regulating Nrf2 and ameliorates murine osteoarthritis. *Food Funct.* **12**, 1590–1602. https://doi.org/10.1039/d0fo02038a (2021).
27. Cao, Y. et al. Extracellular vesicles in infrapatellar fat pad from osteoarthritis patients impair cartilage metabolism and induce senescence. *Adv. Sci.* **11**, e2303614. https://doi.org/10.1002/advs.202303614 (2024).
28. Yilmaz, S., Bedir, E. & Ballar Kirmizibayrak, P. The role of cycloastragenol at the intersection of NRF2/ARE, telomerase, and proteasome activity. *Free Radic. Biol. Med.* **188**, 105–116. https://doi.org/10.1016/j.freeradbiomed.2022.06.230 (2022).
29. Joung, J. et al. Cell enlargement modulated by GATA4 and YAP instructs the senescence-associated secretory phenotype. *Nat. Commun.* **16**, 1696. https://doi.org/10.1038/s41467-025-56929-0 (2025).
30. Dinkova-Kostova, A. T. & Copple, I. M. Advances and challenges in therapeutic targeting of NRF2. *Trends Pharmacol. Sci.* **44**, 137–149. https://doi.org/10.1016/j.tips.2022.12.003 (2023).
31. Bolduc, J. A., Collins, J. A. & Loeser, R. F. Reactive oxygen species, aging and articular cartilage homeostasis. *Free Radic. Biol. Med.* **132**, 73–82. https://doi.org/10.1016/j.freeradbiomed.2018.08.038 (2019).
32. Wei, P. & Bao, R. Intra-articular mesenchymal stem cell injection for knee osteoarthritis: Mechanisms and clinical evidence. *Int. J. Mol. Sci.* https://doi.org/10.3390/ijms24010059 (2022).
33. Lu, J. et al. Intraarticular injection of the stromal vascular fraction for the treatment of knee osteoarthritis a prospective randomized controlled clinical trial. *Sci. Rep.* **15**, 28109. https://doi.org/10.1038/s41598-025-09398-w (2025).
34. Jeyaraman, N. et al. Challenges in the clinical translation of stromal vascular fraction therapy in regenerative medicine. *World J. Stem Cells* **17**, 103775. https://doi.org/10.4252/wjsc.v17.i6.103775 (2025).
35. Baek, J. H., Lee, S. C., Lee, D. N., Ahn, H. S. & Nam, C. H. Effectiveness and complications of bone marrow aspirate concentrate in patients with knee osteoarthritis of Kellgren–Lawrence grades II–III. *Medicina (Kaunas)* https://doi.org/10.3390/medicina60060977 (2024).
36. Xie, J. et al. Sustained Akt signaling in articular chondrocytes causes osteoarthritis via oxidative stress-induced senescence in mice. *Bone Res.* **7**, 23. https://doi.org/10.1038/s41413-019-0062-y (2019).
37. Kang, C. et al. The DNA damage response induces inflammation and senescence by inhibiting autophagy of GATA4. *Science* **349**, aaa5612. https://doi.org/10.1126/science.aaa5612 (2015).
38. Antero, S., Anu, K. & Kai, K. Emerging role of NF-κB signaling in the induction of senescence-associated secretory phenotype (SASP). *Cell. Signal.* https://doi.org/10.1016/j.cellsig.2011.12.006 (2011).
39. Yuchen, C. et al. Control of the senescence-associated secretory phenotype by NF-κB promotes senescence and enhances chemosensitivity. *Genes Dev.* https://doi.org/10.1101/gad.17276711 (2011).
40. Cuadrado, A. et al. Therapeutic targeting of the NRF2 and KEAP1 partnership in chronic diseases. *Nat. Rev. Drug Discov.* **18**, 295–317. https://doi.org/10.1038/s41573-018-0008-x (2019).
41. Wang, L. & He, C. Nrf2-mediated anti-inflammatory polarization of macrophages as therapeutic targets for osteoarthritis. *Front. Immunol.* **13**, 967193. https://doi.org/10.3389/fimmu.2022.967193 (2022).
42. Chen, H. et al. Rhoifolin ameliorates osteoarthritis via the Nrf2/NF-κB axis: In vitro and in vivo experiments. *Osteoarthr. Cartil.* **30**, 735–745. https://doi.org/10.1016/j.joca.2022.01.009 (2022).
43. Qiao, J. et al. ASA VI controls osteoarthritis in mice by maintaining mitochondrial homeostasis through sirtuin 3. *Int. Immunopharmacol.* **140**, 112858. https://doi.org/10.1016/j.intimp.2024.112858 (2024).
44. Zhang, Y. & Ross, A. C. Retinoic acid and the transcription factor MafB act together and differentially to regulate aggrecan and matrix metalloproteinase gene expression in neonatal chondrocytes. *J. Cell. Biochem.* **114**, 471–479. https://doi.org/10.1002/jcb.24387 (2013).
45. Miyamoto, S. et al. Intra-articular injection of mono-iodoacetate induces osteoarthritis of the hip in rats. *BMC Musculoskelet. Disord.* **17**, 132. https://doi.org/10.1186/s12891-016-0985-z (2016).
46. Kwon, M., Nam, D. & Kim, J. Pathological characteristics of monosodium iodoacetate-induced osteoarthritis in rats. *Tissue Eng. Regen. Med.* **20**, 435–446. https://doi.org/10.1007/s13770-023-00520-5 (2023).
47. Zhang, R. et al. Curcumin supplementation enhances bone marrow mesenchymal stem cells to promote the anabolism of articular chondrocytes and cartilage repair. *Cell Transplant.* **30**, 1–12. https://doi.org/10.1177/0963689721993776 (2021).

Author contributions

Study design: M.T. and J.C. Study conduct and data collection: S.H.Z., Y.L.Z. Data analysis: J.D.L. and Y.L.Z. Data interpretation: Y.F.W. Drafting the manuscript: S.H.Z. Funding acquisition: S.H.Z and M.T. All authors have read and approved the final manuscript.

Funding

This study was supported by the 2024QNXM052 (Joint Medical Scientific Research Project of Chongqing Municipal Health Commission and Technology Bureau).

Declarations

Competing interests

The authors declare no competing interests.

Additional information

Supplementary Information The online version contains supplementary material available at https://doi.org/10.1038/s41598-026-43064-z.

Correspondence and requests for materials should be addressed to J.C. or M.T.